DOI: 10.1002/adem.200500212

Creation of Porous Ceria by Sublimation of Tin Dioxide during Sintering**

By *Ying Liu*, and *Meilin Liu**

Porous structures play a crucial role in many applications such as medical implants,[1,2] heat insulation and/or thermal shock resistant structures,[3] chemical catalysis,[4] water purification,[5] gas separation,[6] sensors,[7] and fuel cells.[8,9] Many different strategies have been adopted to control morphology, size and size distribution, the total volume, and connectivity of the voids in porous materials. Template method is one of the most effective approaches for creating pores with desired size and geometry. It has been successfully used to produce uniform porous nanostructures (e.g. nanotubes and honeycombs).[10–12]

A variety of porous microstructures can be created by controlled sintering of particles. The degree of sintering depends on sintering temperature, time, atmosphere, pressure, and the type and amount of sintering additives.[13]

An interesting methodology for creating desired level of porosity is found in the fabrication of solid oxide fuel cell (SOFC) anodes, where porosity is created by the volume change occurred when NiO is reduced to Ni metal.[14] To fabricate SOFC anodes, a mixture of NiO and an electrolyte (YSZ or GDC) powders are fired at high temperatures to achieve desired microstructure and strength. Upon exposure to a reducing atmosphere (e.g., fuels for SOFCs), NiO is reduced to metallic Ni, creating porosity of about 1/3 of the volume fraction of NiO phase in the composite. The porosity of the cermet is thus determined by the ratio of NiO to YSZ (or GDC) and the degree of sintering. If the NiO-electrolyte composite is sintered to full density, the porosity of the cermet is limited to about 1/3 of the volume fraction of NiO phase in the composite.

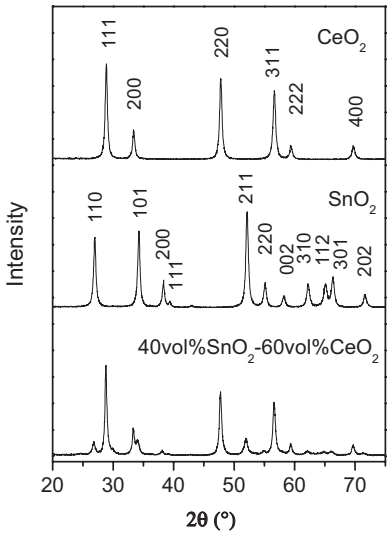

Fig. 1. X-ray diffraction (XRD) patterns of the as-prepared SnO_2, CeO_2, and SnO_2-CeO_2 nanocomposite powders.

Larger porosity can be achieved by adding so-called "pore formers" (usually carbon or cellulose).[15–18] These pore formers occupy some space during the shape forming stages such as tape-casting or dry pressing. They are burned off in the earlier stages of sintering. Sometimes distortion or even collapse of the host material is observed after the removal of pore formers but before firing to desired microstructure and strength, especially when large amount of pore formers is used. In addition, these types of pore formers are not suitable for fabrication processes involving high temperature or high energy for initial shape formation, such as plasma pyrolysis and laser ablation.

To avoid this problem, ceramic "pore formers" such as ZnO are chosen to replace the more commonly used carbon and hydrocarbons. In this method, two immiscible oxide phases (the host material and the pore former) are intimately mixed together and fired to full density. One component is then selectively leached out chemically or by reduction/evaporation, leaving equal amount of porosities in the host material.[19–23] While the feasibility has been demonstrated, these processes are often cumbersome and problematic. For example, the time required for chemical leaching can be as long as 72 hs and additional gas reduction may be necessary.[19] Moreover, contamination or partial reduction of host materials may occur in chemical etching or reduction.

Here we demonstrate an alternative method to prepare highly porous CeO_2 without chemical etching or reduction. It is well known that CeO_2 is an important material for solid state electrochemical applications such as solid oxide fuel

[*] *Dr. Y. Liu*
Current contact address
GE Energy, Hybrid Power Generation Systems
19310 Pacific Gateway Drive
Torrance, CA 90502-1031, USA
E-mail: ying2.liu@ge.com
Prof. M. Liu
Center for Innovative Fuel Cell and Battery Technologies
School of Materials Science and Engineering
Georgia Institute of Technology
Atlanta, GA 30332-0245, USA
E-mail: meilin.liu@mse.gatech.edu

[**] *This work was supported by DOE-SECA (DE-FC26-02NT41572) and by the Center for Innovative Fuel Cell and Battery Technologies, Georgia Institute of Technology. The authors would like to acknowledge the technical assistance from nGmat Co.*

cells, gas separation, and gas sensors. SnO_2 was chosen as a ceramic "pore former" after a careful survey of many potential metal oxides. First of all, SnO_2 and CeO_2 are immiscible. Secondly, neither crystal structure nor the catalytic properties of CeO_2 are influenced by the presence of SnO_2. Thirdly, the melting point of SnO_2 (1630 °C) is near the typical firing temperatures of CeO_2 (usually 1350 ~ 1500 °C) and, thus, SnO_2 phase can be removed by sublimation during firing process without further chemical leaching or gas reduction. Furthermore, the high sublimation temperature of SnO_2 will prevent distortion or collapse of the host material during firing, which is a potential problem when low temperature "pore formers" are used. In this study, CeO_2-SnO_2 nano-composite powder was synthesized using a combustion CVD process from a single precursor solution. SnO_2 phase was then evaporated during high temperature sintering, leaving behind open porous matrix of CeO_2. Neither chemical leaching nor gas reduction is necessary for this new approach. This simple method has great potential for preparation of porous materials for many applications such as solid oxide fuel cells, gas sensors, gas separation, and chemical catalysis.

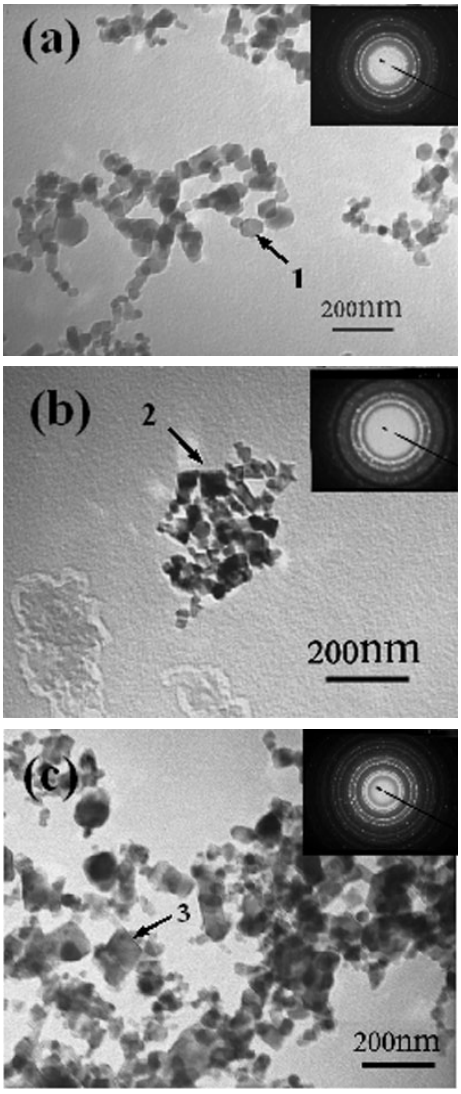

Fig. 2. TEM bright field images and the corresponding selected area electron diffraction (SAED) patterns of the as-prepared nanopowders. (a) SnO_2, (b) CeO_2, (c) 40 vol.% SnO_2-60 vol.% CeO_2 composite.

Shown in Figure 1 are X-ray diffraction (XRD) patterns of the as-prepared SnO_2, CeO_2, and 40 vol.%SnO_2-60 vol.%CeO_2 composite powder. The strong intensity of the peaks indicated that the sample powder was fully crystallized. CeO_2 powder can be indexed to a cubic fluorite structure with lattice constant a = 5.411 Å (JCPDS card # 43-1002). SnO_2 powder was identified as a tetragonal rutile structure with a = 4.738 Å and c = 3.187 Å (JCPDS card # 41-1445). In the XRD pattern for 40 vol.%SnO_2-60 vol.%CeO_2 composite powder, the distinct peaks of individual CeO_2 and SnO_2 phases are observed, further confirming that the two phases are immiscible. It is noted, however, that the intensities of the peaks corresponding to SnO_2 were much weaker than those of CeO_2 nanopowder. Several factors contribute to the difference in peak intensities of the two phases in the composite: (i) the mass percentage of SnO_2 in the composite was only about 37.5 %, (ii) the atomic scattering factor of Ce is larger than that of Sn, (iii) the multiplicity factor of each crystallographic plane for CeO_2 (cubic structure) is greater than that for SnO_2 (tetragonal). For example, in CeO_2, (200), (020), and (002) planes are equivalent and contribute to a single peak on the XRD pattern. In SnO_2, however, (200) and (020) are equivalent planes, but different from (002). Thus more and weaker peaks are observed on SnO_2 XRD pattern than on CeO_2 pattern.

Shown in Figure 2 are TEM images (bright field) of SnO_2, CeO_2 and 40 vol.%SnO_2-60 vol.%CeO_2 composite powder. The insets are the corresponding selected area electron diffraction (SAED) patterns, indicating that all samples were highly crystallized. SnO_2 particles (20 to 50 nm) had a polygonal morphology, as shown in Figure 2(a). In contrast, CeO_2 powder had about the same size but showed a parallelogrammic shape, as shown in Figure 2(b). Both SnO_2 and CeO_2 particles with their distinct morphologies can be seen for the image for a 40 vol.%SnO_2-60 vol.%CeO_2 composite sample shown in Figure 2(c). For free grown crystalline particles, their surfaces usually are less energetic, low index compact planes. For tetragonal SnO_2, planes are the most compact ones (noting lattice constant c is less than a and b for SnO_2). The interplanar angle between {101} planes is calculated to be 95.8°. This is in good agreement with our TEM observations as shown in Figure 2(a) (e.g. particle 1). CeO_2 has a cubic structure. The angle between its most compact planes, {111}, is 70.5° (or 109.5°) (see particle 2 in Fig. 2(b) and particle 3 in Fig. 2(c)).

SnO_2 and CeO_2 nanopowders prepared separately via combustion CVD were mixed together in volume ratio of 40:60 and pressed in a steel die. Figure 3 shows the microstructures of the pellets after sintering and further reduction. Shown in Figure 3(a) is the surface view of a pellet sintered at

ADVANCED ENGINEERING MATERIALS

1450 °C for 5 hs. The average grain size has grown to around 1 μm. Many open pores can be observed on the surface, which could be the consequence of either insufficient sintering or loss of material. Noting the difference of the original particle size (10 nm) and the size of the sintered grains, it is more likely that the partially open microstructure was caused by the sublimation of SnO_2 since the melting points of bulk SnO_2 and CeO_2 are 1630 °C and 2400 °C, respectively.

Shown in Figure 3(b) is a cross-sectional view of the sintered sample. The bottom part is close to the pellet surface. It is noticed more SnO_2 in the surface region than in the inner region has been removed. The more porous region only extended to 30 μm underneath the surface after sintering for 5 hs.

Shown in Figure 3(c) and 3(d) are the surface and internal microstructures of the sintered compacts after being further exposed to a reducing atmosphere (4 %H_2 balanced with argon) at 727 °C for 2 hs. Apparently, SnO_2 phase has been completely removed after reduction in hydrogen, leaving an interconnected, highly open structure with pore size in the range of 0.5 to 1 μm. The porosity of the reduced simples was 39.2 % ± 1.3 %, as determined quantitatively using a stereological imaging analysis technique. The estimated porosity is very close to the volume fraction of SnO_2 in the green sample.

Microstructures of 40 vol.%SnO_2-60 vol.%CeO_2 composite samples prepared from a single precursor source are shown in Figure 4. Both the surface view (Fig. 4(a)) and cross-sectional micrograph (Fig. 4(b)) reveal an extraordinarily open structure. It appears that both the solid phase and the void are interconnected. Shown in Figure 4(c) and 4(d) are the microstructure of the sample after further reduction in hydrogen. No significant changes in microstructure could be observed, implying most of the SnO_2 phase had been completely removed after sintering at 1450 °C for 5 hs. By applying the point-counting technique, porosities of the samples shown in Figure 4(b) and 4(d) were 36.4 % ± 1.8 %, lower than the volume percentage of SnO_2 in the mixture as calculated from the amount of precursors dissolved in the liquid for combustion CVD. The loss of SnO_2 material can be attributed to the high vapor pressure of Sn containing species within the combustion flame.

CeO_2 is a very stable ceramic even at high temperatures under a reducing atmosphere. In contrast, SnO_2 can easily be reduced to tin element and evaporated since the melting point of tin is only 231.93 °C. The Gibbs free energies for CeO_2, SnO_2 and H_2O at 1000 *K* are –1186.134, –666.256, and 448.687 kJ/mol respectively. [24] Thus, CeO_2 cannot

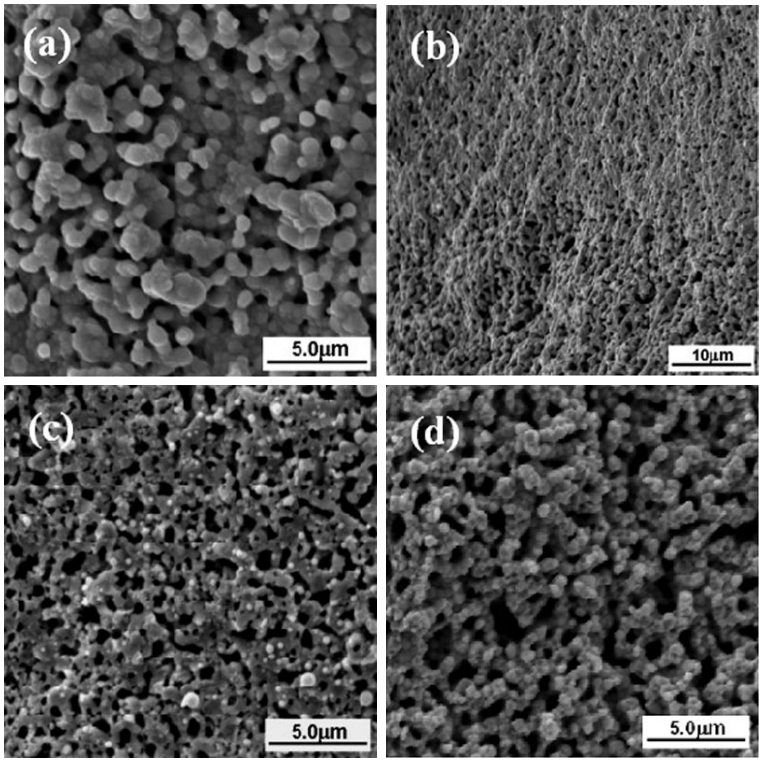

Fig. 3. SEM images of a pellet prepared with 40 vol% SnO_2 – 60 vol% CeO_2 nano-powders. SnO_2 and CeO_2 nano-powders were prepared by combustion CVD separately and then mixed together. (a) Surface and (b) cross-sectional views of pellet sintered at 1450 °C × 5 hs. (c) Surface and (d) cross-sectional views of pellet after reduction at 727 °C × 2 hs.

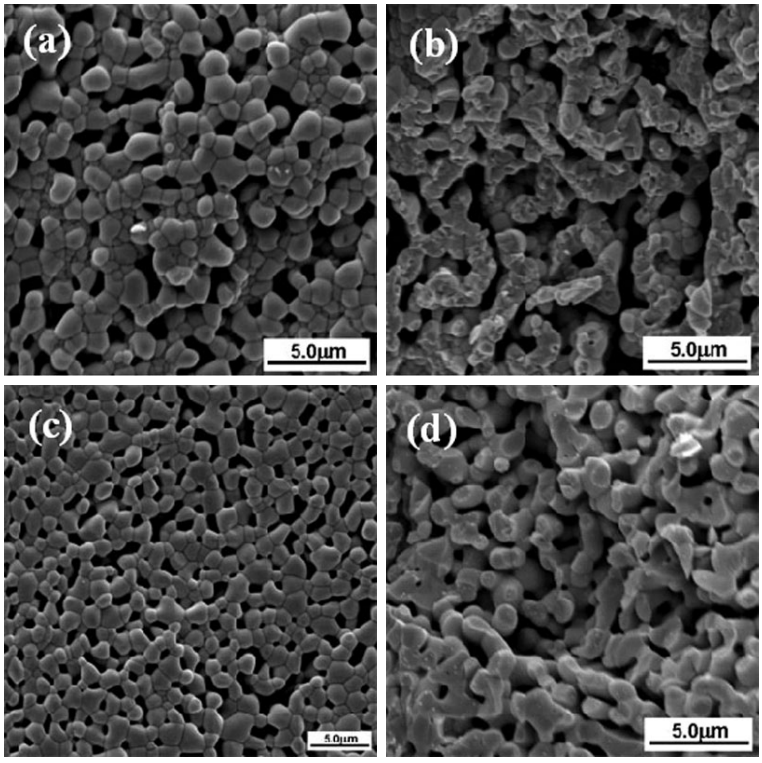

Fig. 4. SEM images of pellet prepared with 40 vol% SnO_2 – 60 vol% CeO_2 nano-powders made by combustion CVD from single precursor solution. (a) Surface and (b) cross-sectional views of pellet sintered at 1450 °C × 5 hs. (c) Surface and (d) cross-sectional views of pellet after reduction at 727 °C × 2 hs.

be reduced to Ce in hydrogen while the reduction of SnO_2 to Sn metal is thermodynamically favored:

$$CeO_2 + 2H_2 = Ce + 2H_2O \qquad \Delta G = 288.76\ kJ/mol \qquad (1)$$

$$SnO_2 + 2H_2 = Sn + 2H_2O \qquad \Delta G = -231.1\ kJ/mol \qquad (2)$$

However, CeO_2 can be partially reduced to Ce_2O_3 at 1000 K.

$$2CeO_2 + 2H_2 = Ce_2O_3 + 2H_2O \qquad \Delta G = -89.89\ kJ/mol \qquad (3)$$

While the reduction of Ce(IV) to Ce(III) and the oxidation of Ce(III) to Ce(IV) are reversible, the redox reactions are accompanied by a volume change that could cause mechanical damage or fracture and thus is detrimental to practical applications.[25]

The difference in removal rate of SnO_2 in the as-prepared and dry-milled 40 vol.%SnO_2-60 vol.%CeO_2 samples during sintering may be attributed to the distribution of SnO_2 phase. Even after long time milling, agglomerates of SnO_2 still exist in the mixture. In contrast, for 40 vol.%SnO_2-60 vol.%CeO_2 sample prepared from a single precursor solution, SnO_2 phase was uniformly distributed throughout the sample.

This simple and cost effective method for preparation of porous ceramic structures is very attractive for many potential applications such as solid oxide fuel cells, solid-state gas sensors, catalysis, and gas separation. In addition, this method can be incorporated into traditional ceramic production routines without introducing additional fabrication procedures. For example, solid oxide fuel cells with porous electrode and dense electrolyte layers could be produced by co-sintering of multiple layer materials. However, some potential limitations associating with this method need to be aware. For example, the hazardous Sn containing gas raises contamination and safety issues to the processing furnaces and the environment. Effective recycling of Sn needs to be studied before this method can be adopted for large scale applications.

We have demonstrated a simple route to preparation of highly porous ceramic structures through the removal of metal oxide (SnO_2) during high temperature sintering. Unlike the existing strategies, the new method requires neither time consuming chemical leaching nor following-up gas reduction procedures. The most critical step for our new approach is the preparation of intimately distributed 40 vol.%SnO_2-60 vol.%CeO_2 composite nanopowder using combustion CVD. This method provides a simple way to introduce additional porosity into ceramic materials, and can be directly incorporate into ceramic production routes without introducing additional procedures.

Experimental

CeO_2-SnO_2 nanocomposite powder was prepared using a combustion CVD process as described elsewhere.[26,27] In this experiment, Sn(II) 2-ethylhexanoate and/or Ce(III) 2-ethylhexanoate (from Strem®) were dissolved in an organic solvent. The solution was sprayed out of an aerosol generating nozzle and combusted with the assistance of methane/oxygen gas mixture. The resulting nanopowder was collected using a specially designed condenser. Three different materials of nanopowders were prepared: SnO_2, CeO_2, and 40 vol.%SnO_2-60 vol.%CeO_2 composite. For the preparation of 40 vol.%SnO_2-60 vol.%CeO_2 composite nanopowder, precursor matrials containing Sn and Ce were dissolved into the same solvent. The resulting single source solution was supplied to the aerosol-generating nozzle. For comparison, SnO_2 and CeO_2 nanopowders were prepared by combustion CVD separately and then mixed together in the volume ratio of 40:60 by dry-milling. Pellet samples were produced by dry-pressing 0.2 g nanopowder in a 10 mm diameter steel die at 250 MPa. The green pellets were fired in a high temperature tube furnace (Lindberg®) at 1450 °C for 5 hs. Some of the samples were heat treated in reducing atmosphere (4 % H_2 balanced with argon) at 727 °C for 2 hs.

Morphologies of the as-prepared nanopowders were characterized using a transmission electron microscope (TEM, JEOL 100C). Crystallographic structures were identified on an X-ray diffractometer (XRD, Phillips PW-1800) at a scanning step of 0.01°/min. Sintered samples were observed under a scanning electron microscope (SEM, Hitachi S-800) equipped with an energy dispersive spectroscopy (EDS) attachment. Porosity of the sintered and reduced samples was calculated using point-counting technique.[28] To make sure an unbiased statistical result, each ceramic sample was broken into smaller pieces, three of which with fresh fractured surfaces were employed for further SEM analysis. At least 20 representative SEM micrographs were acquired randomly for each group of fractured samples. The SEM images were then overlaid with a grid of 169 evenly spaced counting points. The number of test points falling on the voids was counted and divided by the total grid points. This ratio is defined as point fraction (P_p). Volume fraction of the voids (V_v) was estimated by averaging P_p over 20 random microstructural fields:

$$V_v = \langle P_p \rangle \pm \frac{2\sqrt{S^2}}{\sqrt{N}} \qquad (4)$$

where

$$\frac{2\sqrt{S^2}}{\sqrt{N}}$$ formula 1

is the sampling error in the volume fraction determination, N is the total number of microstructural fields, and S is the standard deviation, which was calculated as follows:

$$S^2 = \frac{\sum(\langle P_p \rangle - P_{Pi})^2}{(N-1)} \qquad (5)$$

where P_{Pi} is the point fraction of the ith microstructural field (i=1,2,...n).

Received: September 23, 2005
Final version: October 11, 2005

[1] Y. Z. Yang, J. M. Tian, J. T. Tian, Z. Q. Chen, X. J. Deng, D. H. Zhang, *J. of Biomed. Mater. Res.* **2000**, *52*, 333.
[2] A. Tampieri, G. Celotti, S. Sprio, A. Delcogliano, S. Franzese, *Biomaterials* **2001**, *22*, 1365.
[3] K. Maca, P. Dobsak, A. R. Boccaccini, *Ceram. Int.* **2001**, *27*, 577.
[4] C. D. Wu, A. *Hu*, L. Zhang, W. B. Lin, *J Am. Chem. Soc.* **2005**, *127*, 8940.
[5] M. Arkas, D. Tsiourvas, C. M. Paleos, *Chem. Mater.* **2005**, *17*, 3439.
[6] S. Uemiya, T. Matsuda, E. Kikuchi, *J. Membr. Sci.* **1991**, *56*, 315.
[7] Y. Liu, E. Koep, M. Liu, *Chem. Mater.* **2005**, *17*, 3997.
[8] S. C. Singhal, K. Kendall, *High Temperature Solid Oxide Fuel Cells : Fundamentals, Design, and Appl.* Elsevier, Oxford **2003**.
[9] N. Q. Minh, T. Takahashi, *Sci. and Technol. of Ceram. fuel Cells*, Elsevier, The Netherlands **1995**.

[10] B. B. Lakshmi, P. K. Dorhout, C. R. Martin, *Chem. Mater.* **1997**, *9*, 857.
[11] J. H. He, T. Kunitake, T. Watanabe, *Chem. Commun.* **2005**, 795.
[12] J. S. Jie, G. Z. Wang, Q. T. Wang, Y. M. Chen, X. H. Han, X. P. Wang, J. G. Hou, *J. of Phys. Chem. B* **2004**, *108*, 11976.
[13] S. Maschio, A. Bachiorrini, E. Lucchini, S. Bruckner, *J. Europ. Ceram. Soc.* **2004**, *24*, 3535.
[14] C. Xia, M. Liu, *Solid State Ionics* **2001**, *144*, 249.
[15] R. J. Gorte, J. M. Vohs, *J. Catal.* **2003**, *216*, 477.
[16] J. J. Haslam, A. Q. Pham, B. W. Chung, J. F. DiCarlo, R. S. Glass, *J. Am. Ceram. Soc.* **2005**, *88*, 513.
[17] C. S. Kong, D. Y. Kim, H. K. Lee, Y. G. Shul, T. H. Lee, *J. Power Sources* **2002**, *108*, 185.
[18] N. Koc, M. Timucin, F. Korkusuz, *Ceram. Int.* **2004**, *30*, 205.
[19] E. S. Toberer, A. Joshi, R. Seshadri, *Chem. Mater.* **2005**, *17*, 2142.
[20] E. S. Toberer, J. C. Weaver, K. Ramesha, R. Seshadri, *Chem. Mater.* **2004**, *16*, 2194.
[21] M. Panda, R. Seshadri, J. Gopalakrishnan, *Chem. Mater.* **2003**, *15*, 1554.
[22] M. Panda, M. Rajamathi, R. Seshadri, *Chem. Mater.* **2002**, *14*, 4762.
[23] M. Rajamathi, S. Thimmaiah, P. E. D. Morgan, R. Seshadri, *J. Mater. Chem.* **2001**, *11*, 2489.
[24] I. Barin, *Thermochi. Data of Pure Substances*, VCH, New York **1995**.
[25] S. P. S. Badwal, F. T. Ciacchi, J. Drennan, *Solid State Ionics* **1999**, *121*, 253.
[26] Y. Liu, W. Rauch, S. Zha, M. Liu, *Solid State Ionics* **2004**, *166*, 261.
[27] Y. Liu, S. Zha, M. Liu, *Adv. Mater.* **2004**, *16*, 256.
[28] R. T. DeHoff, F. N. Rhines, *Quantitative Microsc.* McGraw-Hill Book Company, New York **1968**.

DOI: 10.1002/adem.200500198

Microstructural Bases for the Superior Densification of Gels doped with Alumina Nanoseeds**

By *Jesus Tartaj* and *Pedro Tartaj**

Alumina in its different forms has found applications in a broad variety of technological fields from catalysis to the electronic industry and from synthesis to biomedical applications.[1] The bases for this outstanding multifunctionality of alumina reside on the special properties of its different phases. For example, α-Al_2O_3 is bioinert, it exhibits high elastic modulus, thermal and chemical stability, high strength and toughness, and excellent dielectric properties. Some of these properties are extremely dependent on particle dimensions and are expected to improve when reducing particle size down below the microscale.[2] Different routes have been used to produce α-Al_2O_3,[3–6] among which the sol-gel routes have been shown to have the potential to keep the particle size below the microscale after densification. However, isostructural seed particles must be added to the initial gels to avoid the high temperatures required for their densification (i.e. to avoid significant grain coarsening).[5–7]

We have recently reported that a novel sol-gel self-production method for α-Al_2O_3 nanoseeds is adequate for the production of high-densified α-Al_2O_3 materials at relatively low temperatures.[8] The success of this method resides upon the addition of isostructural nanoparticles (obtained from a low-cost raw material pseudoboehmite) to the initial gels. Ultimately, density, grain size, pore size, and defects dictate the properties of ceramics, which makes appropriate to carry out a detailed study about the events responsible for the reduction of densification temperatures upon the addition of different amount of nanoseeds. Thus, the issue of this work is to

[*] *Dr. J. Tartaj*
Electroceramics Department
Instituto de Cerámica y Vidrio (CSIC)
Camino de Valdelatas s/n
Cantoblanco, 28049 Madrid, Spain
E-mail address: jtartaj@icv.csic.es
Dr. P. Tartaj
Particulate Materials Department
Instituto de Ciencia de Materiales de Madrid (CSIC)
Cantoblanco, 28049 Madrid, Spain
E-mail address: ptartaj@icmm.csic.es

[**] *P. Tartaj thanks the financial support from the Ramon y Cajal program.*

